Study of the Head Loss Associated with a Fluid Flowing through a Porous Screen

Channing R.C. Santiago, REU Student
Ted Chu, Graduate Mentor
and
K. H. Wang, Faculty Mentor

Final Report

Department of Civil and Environmental Engineering
University of Houston
Houston, Texas

Sponsored by the National Science Foundation
REU Program

August 2007

Abstract

An experimental investigation of water flowing through a porous screen in an open channel was conducted to better understand the mechanism of energy loss and associated influence factors in a system with fluid flowing through porous screens. The screens selected for this study are perforated screens with circular hole of different size and porosity. By recording the upstream and downstream water depths with distinct screens at different flow rates and screen inclinations, a series of mathematical formulas were derived to represent each of these factors' influence on the calculation of the energy loss.

Introduction

The porous screens are commonly used in fluid domain to restrict objects from further advancing. The applications include diverting fish from entering the pump intakes, removing debris from an intake of a cooling system connected to a power plant, and capturing solid wastes in a waste water treatment plant. The porous structures can also be applied to dissipate wave energy for preventing from direct wave impact in coastal areas.

An important phenomenon that occurred during the process of fluid flowing through a porous structure is the energy loss or termed head loss. Part of the energy losses are caused by the friction of the opening holes as fluid passing through them and the other part of energy losses are the result of the turbulence enhanced energy dissipation behind the porous structure. For the design and application purpose, it is essential to find ways in estimating the total energy losses under conditions that fluids

flow through a porous structure. The head loss for flow passing through a wedge wire screen was studied experimentally by Yeh and Shrestha (1990). Wang (2004) conducted a series of extensive tests to measure the head losses for screens used in waste water treatment plants. The screens tested include bar screens with various bar spacing, perforated screens of different pore size, stepped screens and others.

Screen induced head loss can be measured straightforwardly in a setup of an open channel flow. In this study, experimental measurements were carried out to determine the head losses for four perforated screens of various pore sizes placed in selected four angles of inclination. The data for each screen head loss-test were collected under various flow rate conditions. All data gathered served as a basis to understand the fundamental properties of porous screens that affect the head loss and used to eventually derive empirical formulas to estimate the head loss for screens with a given pore size, porosity, and approaching velocity.

Theoretical Background

The fluid domain is shown in Fig. 1. The fluid is bounded horizontally by the flume floor and the free surface. The upstream depth is represented by Y_1, and Y_2 represents the downstream depth. The screen obstructing the flow is placed at an angle of inclination, θ.

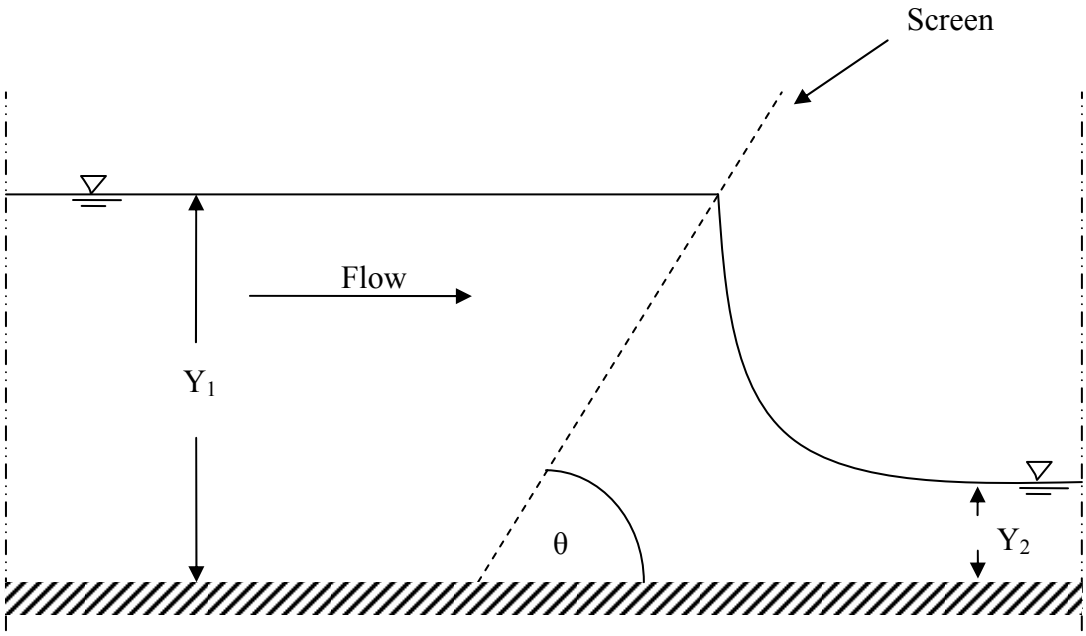

FIG. 1. Diagram of the Fluid Domain

The head loss associated with a fluid flowing through a screen can easily be calculated using the energy equation:

$$\Delta H = Y_1 + \frac{V_1^2}{2g} - \left(Y_2 + \frac{V_2^2}{2g}\right), \quad (1)$$

Where V_1 and V_2 are respectively the uniform velocities for the upstream and downstream cross sections. From the energy equation, we find that head loss is directly proportional to $\frac{V^2}{2g}$. Plotting head loss against $\frac{V^2}{2g}$ for a screen will result in a function describing their relation.

The average pore velocity, V_P, and head loss will also have a distinct relation. Pore velocity is the direct result of the fluid being contracted through the limited open area in a screen. The ratio of the open area provided by the pores to the total area of a given screen is known as porosity. The screens used were cut in a pattern known as a

Round-60º Staggered Center. In order to find the porosity, the diameter of the pores and the length from the center of one pore to the other must be known. The following diagram displays the pattern and equation necessary to determine the porosity.

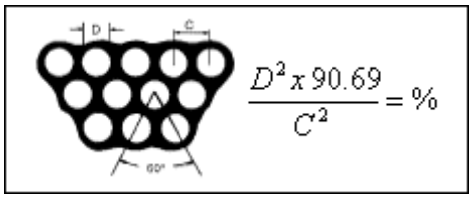

FIG. 2. Diagram of a Round - 60º Staggered Center

———. (2)

With the use of porosity and the continuity equation:

, (3)

the average pore velocity can be derived. The flume used for the tests has a width of 1.0 ft. This would mean $A_1 = Y_1$. In Fig. 3, a fluid is approaching the porous screen with a velocity, V_1, and the porous screen is inclined at an angle, θ. By using a simple trigonometric ratio, the length, S_L, of the submerged area of the screen can be defined as ——. To obtain the open area of the screen, we multiply the porosity of the screen with this area, i.e. $A_p = S_L \phi$. Using these identities, the average pore velocity can be defined as:

— ——— ———. (4)

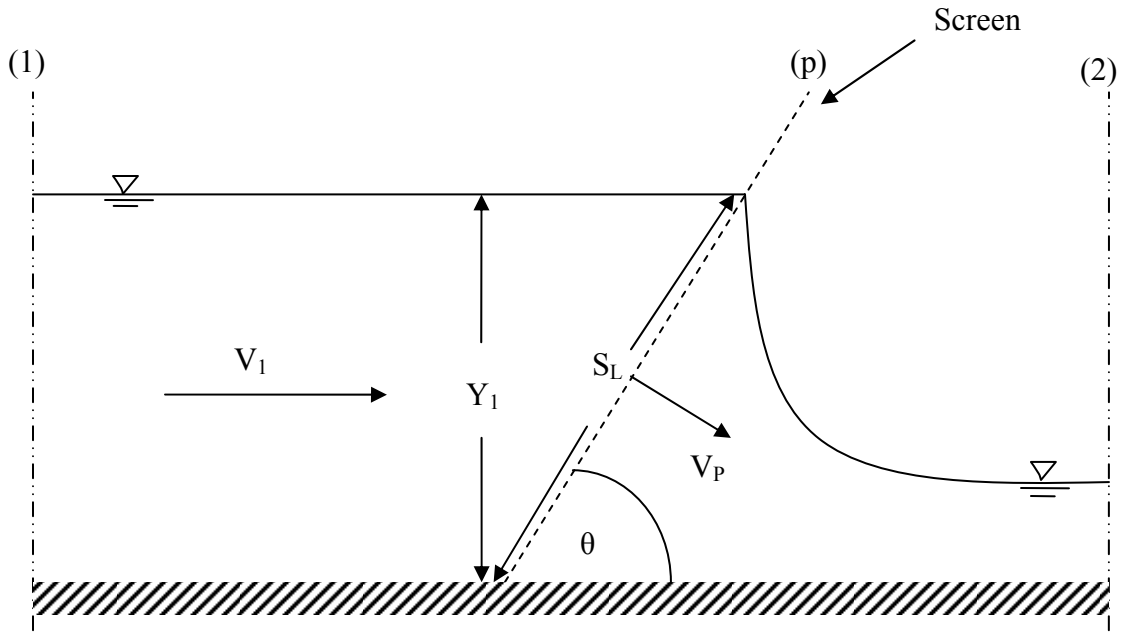

FIG. 3. Derivation of the Average Pore Velocity

Darcy's law has been used to explain the water flow in an aquifer or a porous medium. Using variables defined in Fig. 4, Darcy's law is as described as follows:

$$Q = \frac{-kg}{\nu}\frac{(P_b - P_a)}{L}. \qquad (5)$$

where υ is the kinematic viscosity and k denotes the intrinsic permeability. P_a and P_b are pressures at points a and b, respectively. A is the cross sectional area and L is the length of the porous medium.

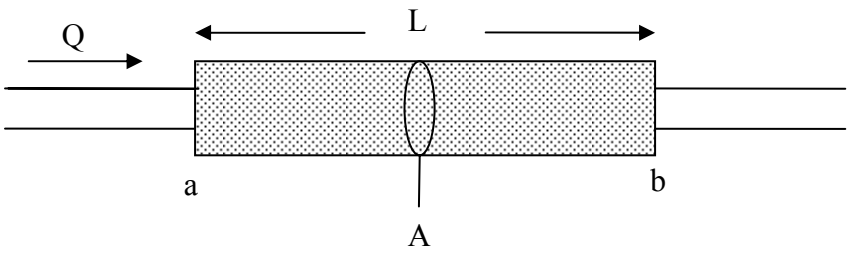

FIG. 4. Diagram Modeling a Darcy's Flow

An aquifer is essentially a porous medium with an extremely low porosity. Darcy's law may, therefore, be able to apply to water flowing through a porous screen depending on the pore size and the approaching velocity. A porous screen will have a behavior following Darcy's law when the Reynolds number based on the approaching velocity and the pore size is small or in this study, it is less than the screen's critical Reynolds number,$R_{e_{cr}}$:

$$R_e = \frac{V_1 d}{\nu} < R_{e_{cr}} . \quad (6)$$

where d is the pore size. However, the critical Reynolds numbers for different screens remain to be determined from the measured data. When the Reynolds number is greater than this critical value, the head loss may follow a non-Darcy flow. This idea was presented by Forchheimer (1901) when he discovered Darcy's law is not valid for all flows through porous media. The following quadratic equation was proposed by Forchheimer (1901) to model this behavior:

$$I = aV + bV^2. \quad (7)$$

Where I is the hydraulic gradient. A similar study was also examined by Venkataraman and Rao (1998). The velocity used in equation (7) can be derived by manipulating Equation (5). When flow satisfies Darcy's law, from Equation (5), we have

$$\frac{(P_a - P_b)}{L} = \nabla P = \frac{\nu}{gk} V, \quad (8)$$

where, V is the discharge velocity (discharge per unit area) and ∇P is the pressure gradient along the flow direction. Comparing Equation (7) with Equation (8), it gives $a = \frac{\nu}{gk}$ and b = 0. Linear regression can be applied to find the coefficients for: (a) a Darcy flow and (b) a non-Darcy flow.

Experiments

A. The Hydraulic Lab and Equipment

The hydraulic lab is equipped with a 25.5-ft long, 1.0-ft wide and 3.0-ft deep rectangular flume of glass walls and horizontal bottom (Fig. 5). The flume is supplied by an elevated head tank and delivers water through a vertical pipe (Fig. 6). The bottom end of the pipe is surrounded by honeycomb boxes to eliminate turbulence as the water proceeds to the flume. The water discharged from the flume is carried in a low-level channel to be pumped back into the head tank and recycled.

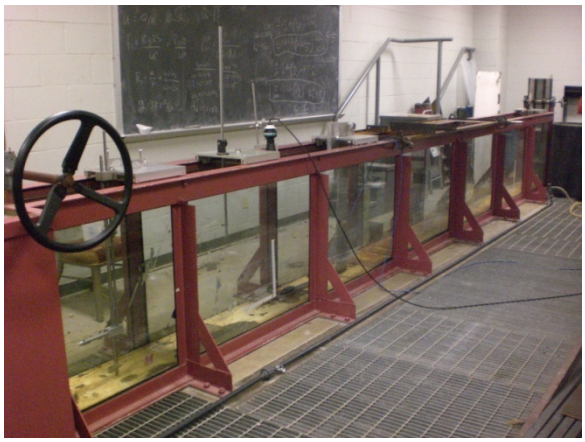

FIG. 5. A 25.5-ft long, 1.0-ft wide and 3.0-ft deep rectangular flume in the Hydraulic Lab

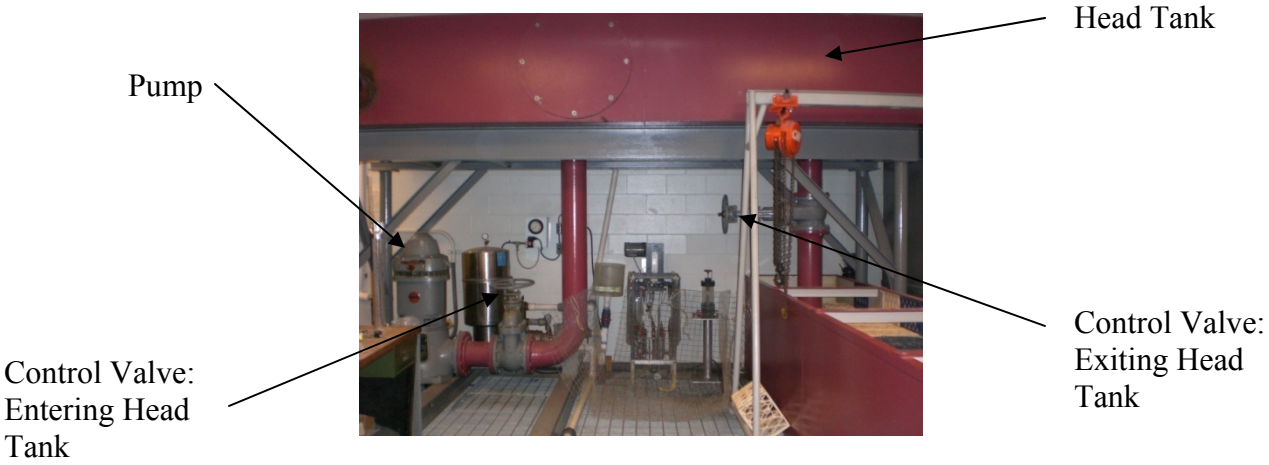

FIG. 6. Head Tank and Control Valves

A constant flow rate was maintained by adjusting the flow control valves located on the pipes entering and exiting the head tank (Fig. 6). The velocity was measured using a *Pulsar Speedy* velocity sensor (Fig. 7). The depth sensor for the water depth measurement was placed at 63-in upstream from the toe of the screen. The *Ultra5* integrates the signals from the velocity and depth sensor and coverts them to the flow rate.

FIG. 7. *Pulsar Speedy* velocity sensor

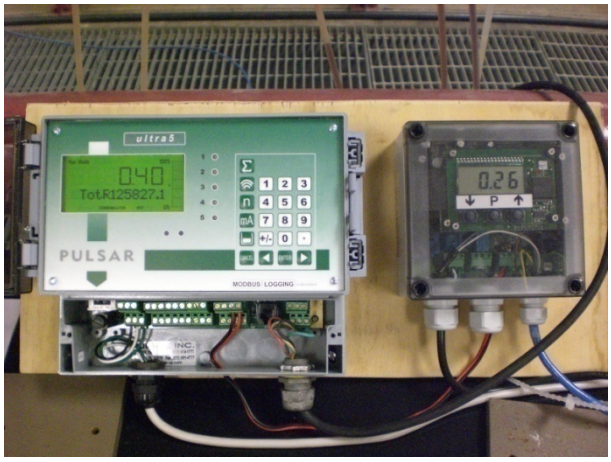

FIG. 8. *Ultra5* integration unit

For calculating head loss, point gages with 1-mm precision were used to measure the water height upstream and downstream of the screen. The upstream point gage was placed approximately 77 inches in front of the screen. To avoid the turbulence, the downstream point gage was placed much further downstream from the screen at approximately 153.5 inches in the uniform flow region.

Four thin, porous screens were tested during the experiment. The first screen (Fig. 9(a)) contained 0.25-in diameter holes with a length of 0.375 inch from center to center

whereas the second screen (Fig. 9(b)) has 0.125-in diameter holes with a length of 0.1875 inch from center to center. Using Equation (2), it was found that the first two screens have the same porosity of 0.4031. For the third and fourth screen (Figs. 10(a) and 10(b)), the diameters of the holes were 0.09375-in and 0.0625-in, and their center-to-center lengths were respectively 0.125-in and 0.1875-in. Again, the derived porosity for the last two screens was found to be the same as 0.2267.

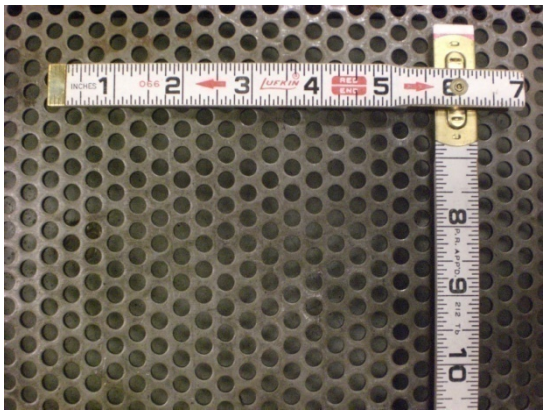

FIG. 9(a). 1/4” Diameter Hole Screen

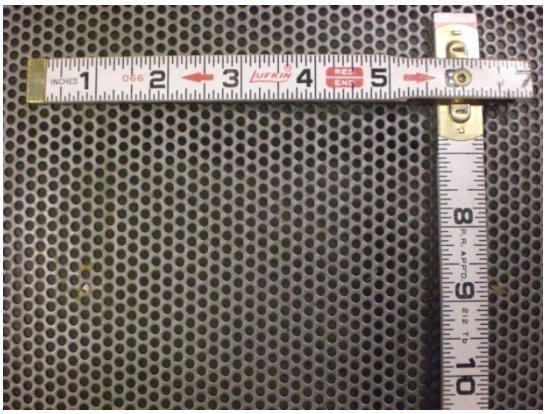

FIG. 9(b). 1/8” Diameter Hole Screen

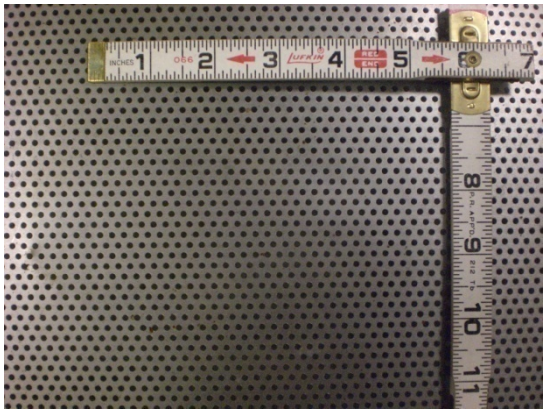

FIG. 10(a). 3/32” Diameter Hole Screen

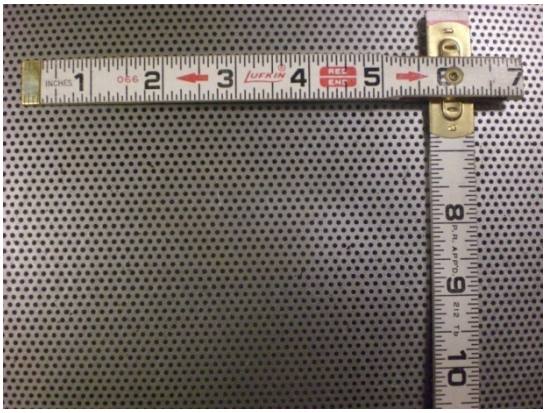

FIG. 10(b). 1/16” Diameter Hole Screen

During the tests, the screens were held in place by an upper and lower brace. The lower steel brace rested on the flume floor and contained slits that were used to insert the foot of the screen. The upper brace consisted of a steel plate that was clamped to the top

of the flume as seen in Fig. 11. The plate had a 74-in x 15-in rectangular opening in the center which had a series of bolt holes running along both sides of the plate. These holes were used to bolt a steel bar running across the top of the channel that held the porous screen in place. Four different pairs of bolt holes were used to lean the porous screen at the desired angle of inclination, θ; the fixed angles used were θ = 90º, θ = 75º, θ = 68º and θ = 59º. At θ = 90º, the screen is orthogonal to the channel floor.

FIG. 11. Upper Brace Supporting the Porous Screen

B. Procedure

The tests for determining head loss through a porous screen at a steady flow condition consists of a total of 12 different flow rates for the screens (1/4”- and 1/8”- hole screens) with a porosity of 0.4031. These flow rates range from 0.10-cfs to 2.20-cfs. With the exception from 0.10-cfs to 0.20-cfs, the flow rates changes in increments of 0.20-cfs. Due to the minor fluctuated nature of free flowing water, the flow rate and velocity were recorded every 30 sec. for a total of 5.0 min. The flow rates and velocities collected for data analysis were an average of these values. The upstream and downstream depths were also recorded in order to be used in the Equation (1) for

determining head loss. At each flow rate, the four selected angles previously mentioned were tested. The screens (3/32”- and 1/16”- hole screens) with a porosity of 0.2267 were tested at flow rates ranging from 0.10-cfs to 1.6-cfs. The braces were unable to support the forces acting on these two screens at flow rates higher than 1.6-cfs, which resulted in fewer flow rates tested. The same increments, between flow rates, used in the screens with a porosity of 0.4031 were used with these flow rates.

C. Behavoir of Flow behind Porous Screens

There was a discrepancy between the envelopes of the free surface that were formed directly behind the screens. In the case of the screens with a porosity of 0.4031, the envelope appeared to have a parabolic decent onto the downstream depth with a smooth surface profile (see Fig. 12). However, for the screens with a porosity of 0.2267, a steeper parabolic free-surface envelope when descending onto the lower depth could be noticed (Fig. 13). The free-surface behind the screen showed amplified fluctuation and the surface was not as smooth as the cases for screens with porosity of 0.4031. The increase of the turbulence intensity reflects the increase of the head loss for the same approaching flow rate. More figures showing test results can be found in Appendix II.

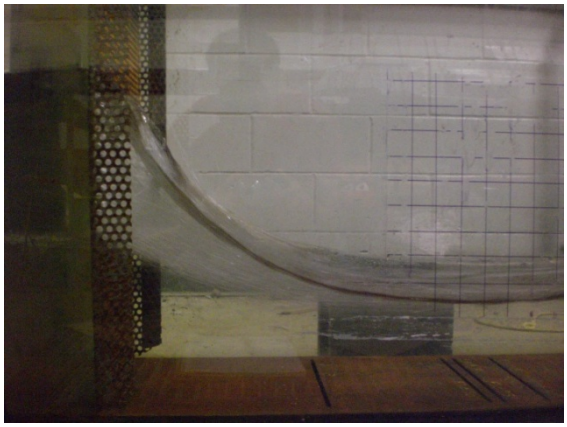

FIG. 12. 1/4” Screen (Porosity-0.4031) at 2.0-cfs

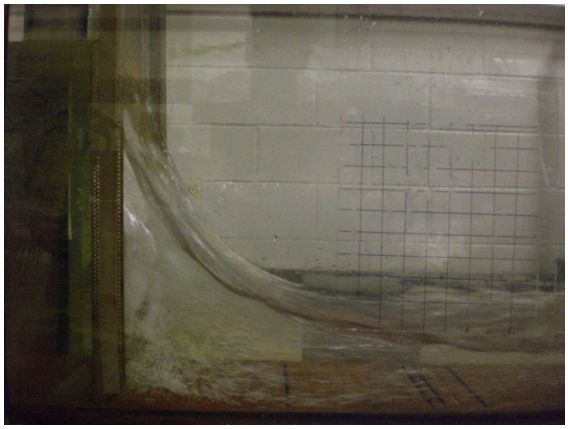

FIG. 13. 1/16” Screen (Porosity-0.2267) at 1.4-cfs

Results

As shown in Fig. 14, with a decreasing flow rate there is a decrease in head loss. The figure also shows that at each flow rate the head loss decreases with decreasing angles of inclination. During analysis, the variation of head loss versus Q^2 was first examined. The head loss for ¼" screen was plotted against $\frac{Q^2}{2g}$ in Fig. 15. The resulting plot indicates the linear variation between head loss and $\frac{Q^2}{2g}$ in the region of large flow rates, and the head loss decrease in a nonlinear trend as flow rate decreases. However, the projected linear line does not reach the origin and it's hard to separate the regions for the Darcy and non-Darcy's flows. It can be seen that $\frac{Q^2}{2g}$ has area as a factor and does not have the dimension of length as the head loss. As a result, this complicates the process of determining an equation to represent the head loss.

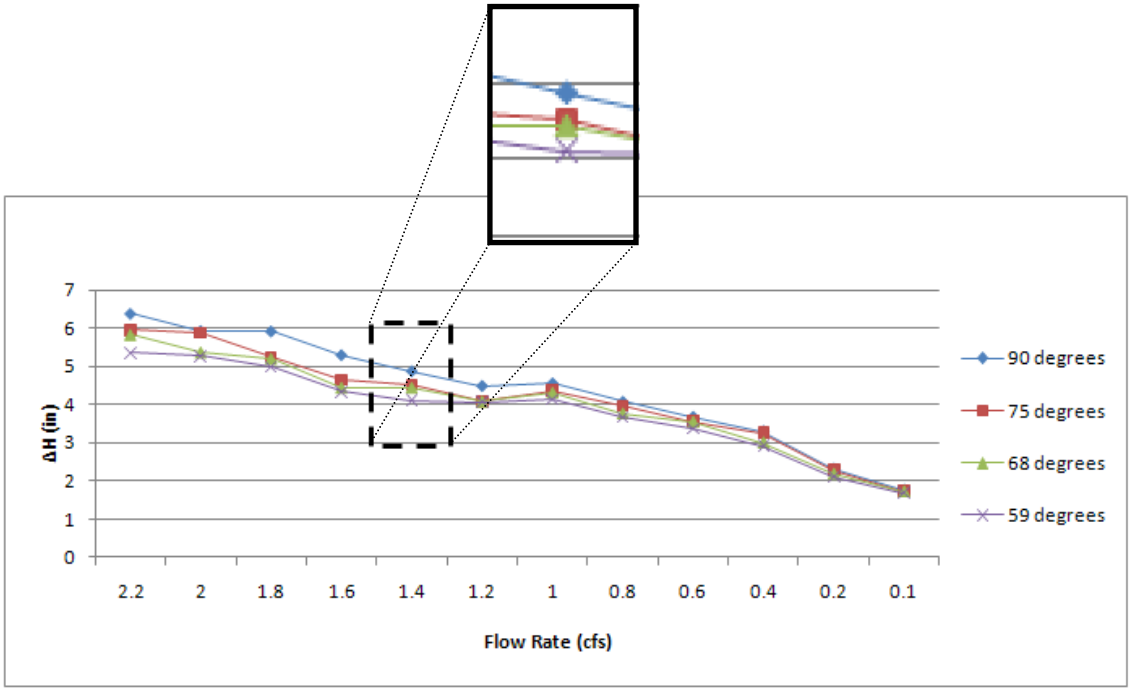

FIG. 14. Head Loss Trend of 0.25" Diameter Hole Screen

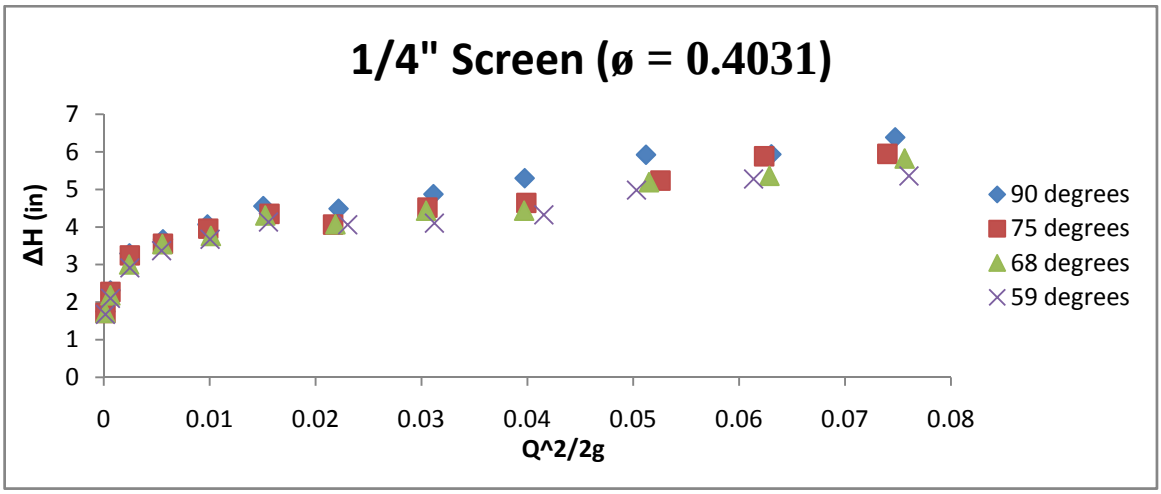

FIG 15. Plot of ΔH vs. $\frac{Q^2}{2g}$

To continue the analysis, head loss for ¼" screen was plotted versus $\frac{V_1^2}{2g}$ as shown in Fig. 16. This plot began to show an apparent transition between the first region (for $\frac{V^2}{2g}$<0.03) data to the second region ($\frac{V^2}{2g}$ ≥ 0.03). For the data in the second region, it clearly reflects the linear variation between head loss and the velocity head, $\frac{V^2}{2g}$. This plot (Fig. 16), however, did not incorporate the screen's angle of inclination. To include the effect

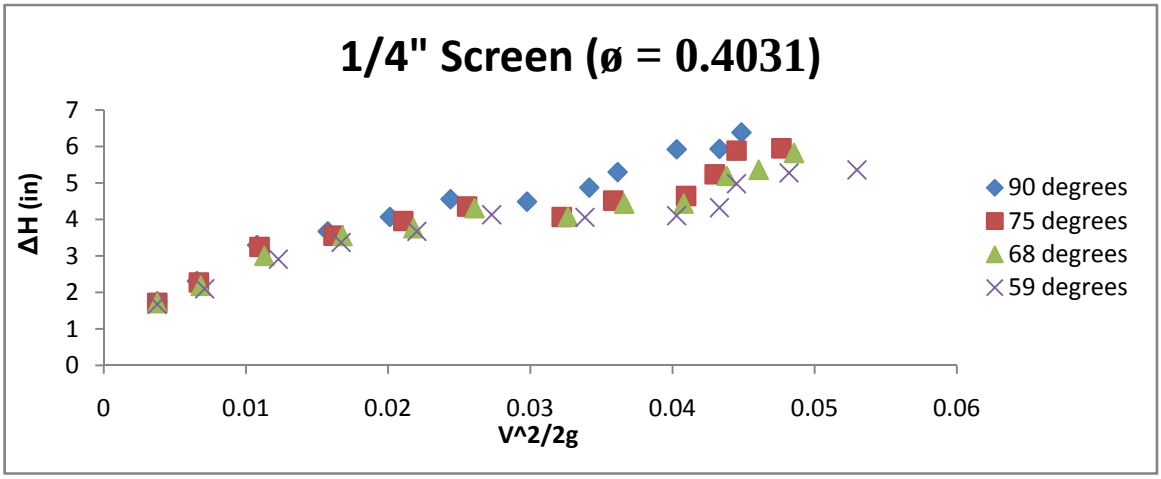

FIG. 16. Plot of ΔH vs. $\frac{V^2}{2g}$

of the screen tilted at angle, θ, the velocity used was changed from the upstream velocity to the velocity normal to the screen. The graph of the head loss plotted against $\frac{(V_1 \sin\theta)^2}{2g}$ is shown in Fig. 17. With this plot, we see that using the normal velocity results in the best correlation between the angles for a certain screen. Comparing with results in Fig. 16, it can be seen all data for different angle of inclination are no longer separated; rather they line up to form a single variation trend. Therefore, the data analyses were conducted with plots between the head loss and $\frac{(V_1 \sin\theta)^2}{2g}$.

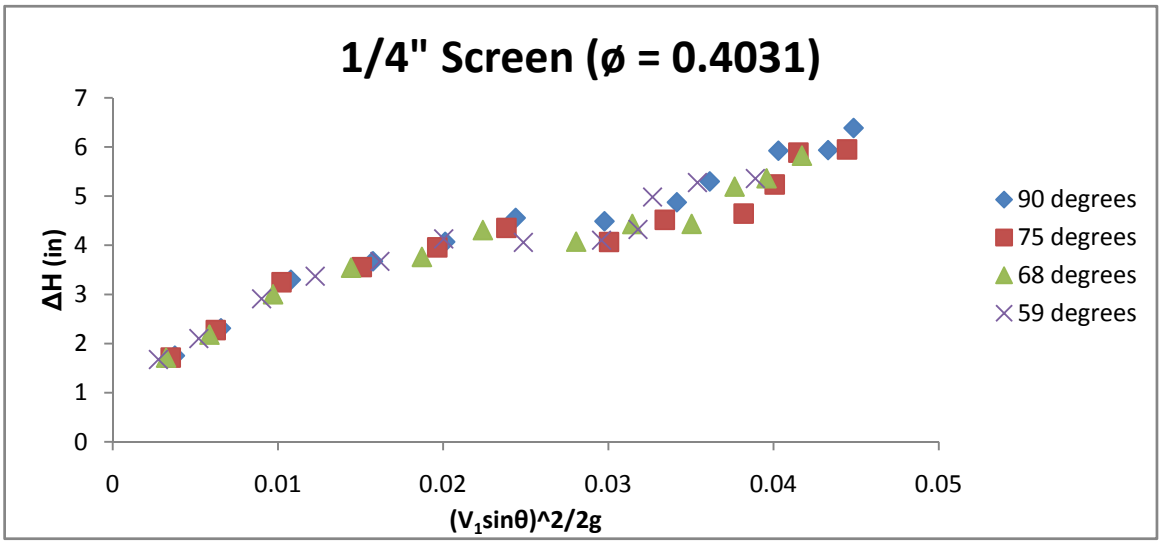

FIG. 17. Plot of Head Loss vs. $\frac{(V_1 \sin\theta)^2}{2g}$

The complete data tested for four screens are presented in Fig. 18, which shows the variation of head loss versus $\frac{(V_1 \sin\theta)^2}{2g}$. It is interesting to note two separated trend of data groups are formed, one is for the two screens with the porosity of 0.4031 (lower group) and the other is for the two screens with porosity of 0.2267 (upper group). From Fig. 18, we notice a similar variation trend can be obtained for screens with the same porosity, although the pore sizes are different. This correlation shows much stronger for

screens with ø = 0.4031. This phenomenon proves that porosity is more of a factor than the pore diameter when it is related to predicting the head loss associated with a fluid flowing through a porous screen. Furthermore, screens with higher porosities appear to have a lower head loss.

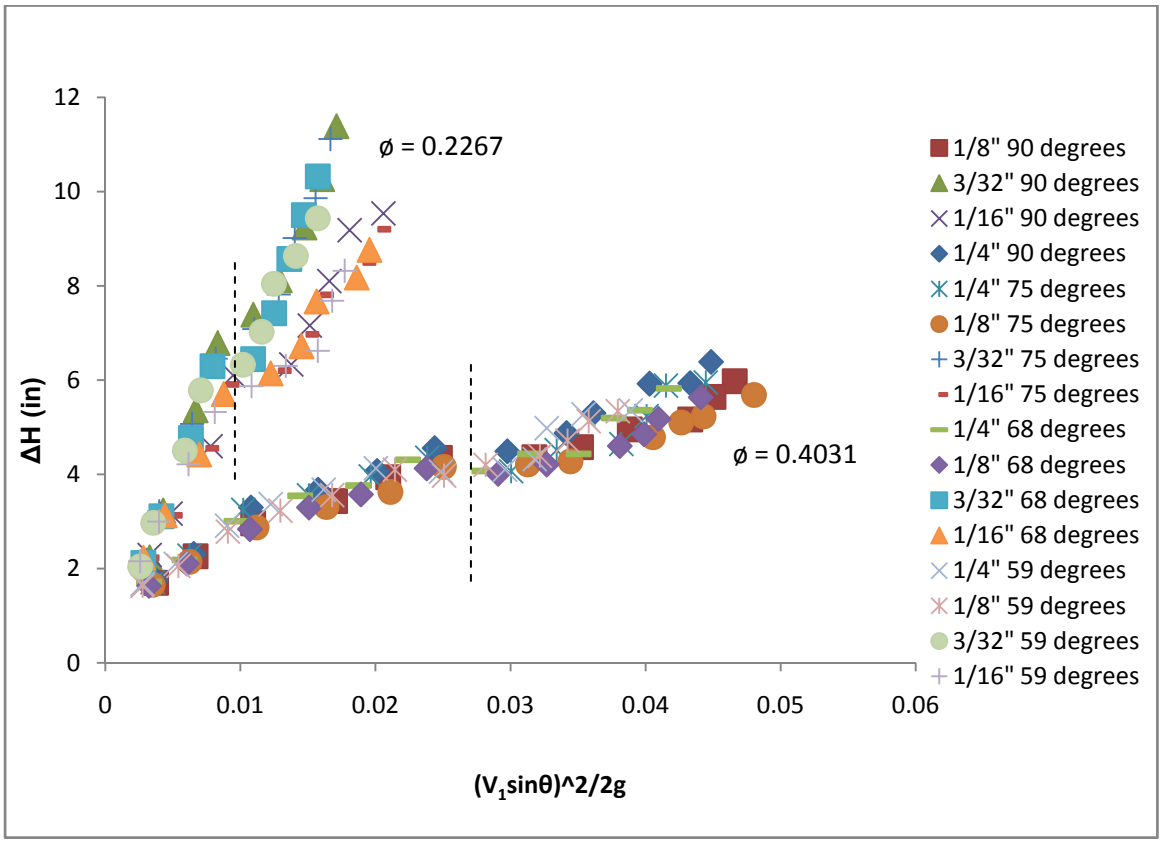

FIG. 18. Full Plot of ΔH vs. $\frac{(V_1 \sin\theta)^2}{2g}$

As shown in Fig. 18, along each data group, there was a noticeable transition between the first region and the second region. These two regions may be separated by a typical Reynolds number defined as critical Reynolds number, $R_{e_{cr}}$. An example of this transition for screens with ø = 0.4031is plotted in Fig. 19. The dash line shows the point separates the two different flow regions. The results reflect the equation proposed by

Forchheimer (1901) for defining Darcy's and non-Darcy's flow regions. To apply Forchheimer's equation and examine the transition from $I = aV$ to $I = bV^2$, the data for

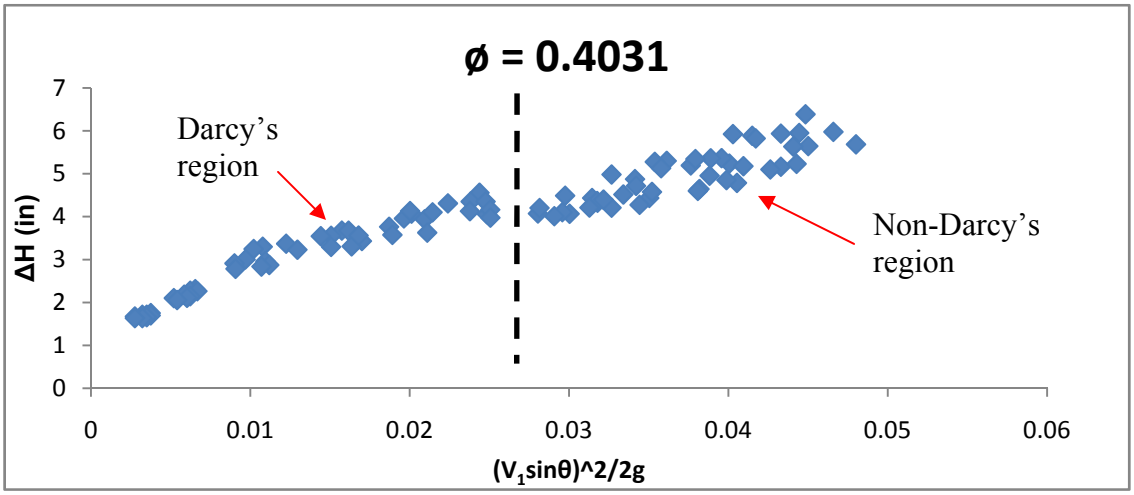

FIG 19. Example of Transition

screens with porosity of 0.4031 were analyzed. Function of power law describing change of head loss versus $\frac{(V_1 \sin\theta)^2}{2g}$ was applied to the first region of the data plotted in Fig. 20. The resulting function was $y = ax^{\frac{1}{2}}$ (with a = 24 and the exponent is about ½). In Fig. 20, the head loss is plotted versus $\frac{(V_1 \sin\theta)^2}{2g}$, which is proportional to V^2. When applied $x = V^2$, the end result shows the head loss is a function V. The flows in this region can be classified as Darcy's flows. So this holds true to the first part of the equation Forchhiemer (1901) proposed as $I = aV$. When linear regression was applied to the second region of the data (shown in Fig. 21), a clear linear function was obtained. The head loss is a function of V^2 and the flow is non-Darcy. This means the second part of Forchhiemer's equation of $I = bV^2$is satisfied. It should be noted the critical Reynolds number separating the Darcy's and non-Darcy's flow regions is about 2000.

Therefore, for screens with porosity of 0.4031, the empirical formula to determine the head loss can be developed as

$$\Delta H = \frac{17 \sin\theta}{\sqrt{g}} V_1 \qquad \text{when } R_e \leq 2000 \quad , \tag{9a}$$

$$\Delta H = 132.8 \sin^2\theta \frac{V_1^2}{2g} \qquad \text{when } R_e > 2000 \quad , \tag{9b}$$

where ΔH is in inches and V_1 is in ft/sec.

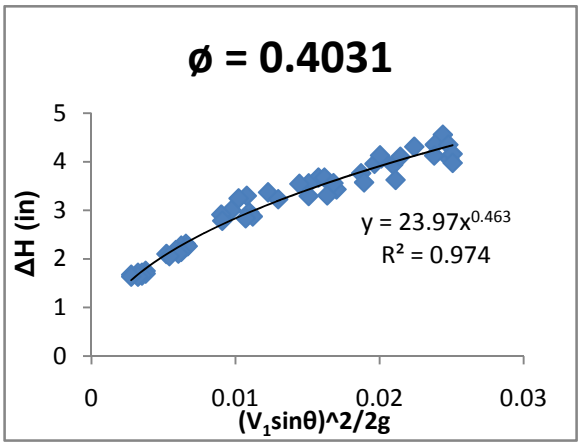

FIG. 20. First region of Data Set for Screens with ø = 0.4031

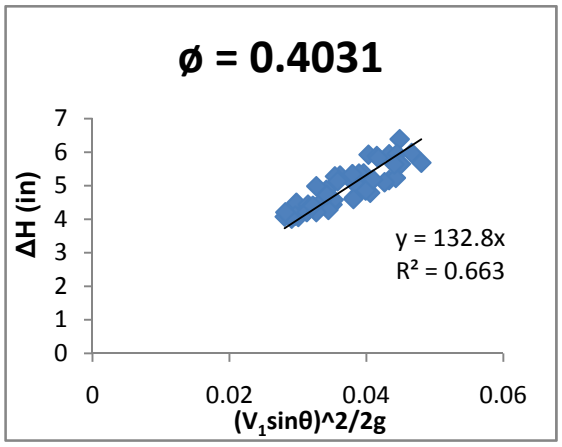

FIG. 21. Second region of Data Set for Screens with ø = 0.4031

The same analyses were applied to the screens with a porosity of 0.2267. In this case, the critical Reynolds number is about 500. The results are shown in Figs. 22-24. The variation trend, however, does not hold in consistency with the results from the screens with porosity of 0.4031. The data in the first region (Fig. 23) do not support the power law function as in the case presented in Fig. 20. It more or less fits in the linear function. We may need to collect more data and test thicker screens to reexamine the flow condition for screens with porosity of 0.2267. For the second region (shown in Fig. 24), even though the data for two screens of different pore sizes show noticeable separation, a linear regression can still be reasonably applied to represent the data. This

indicates the flow in the second region is, as the case presented in Fig. 21, non-Darcy. Certainly more tests will be needed to justify this conclusion.

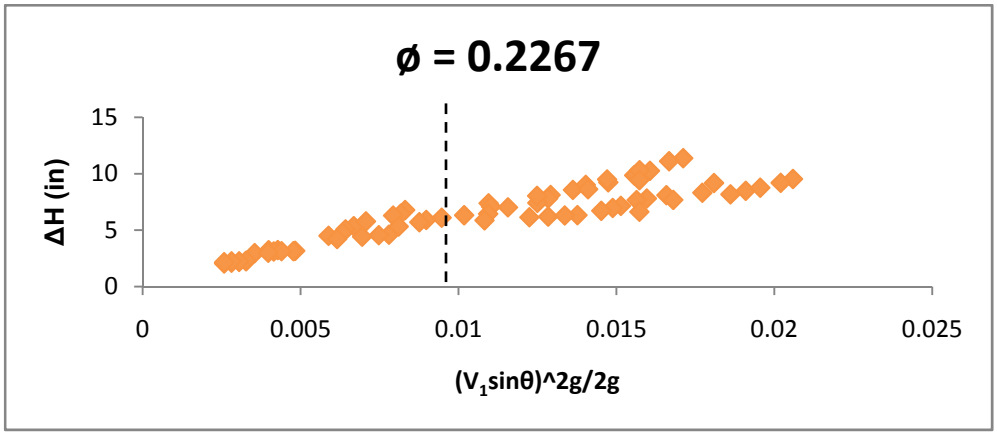

FIG.22. Full Data Plot of Screens with Porosity of 0.2267

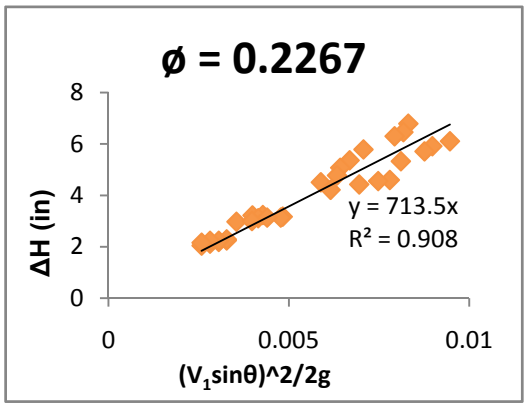

FIG.23. First region of the Data Set for Screens with ø = 0.2267

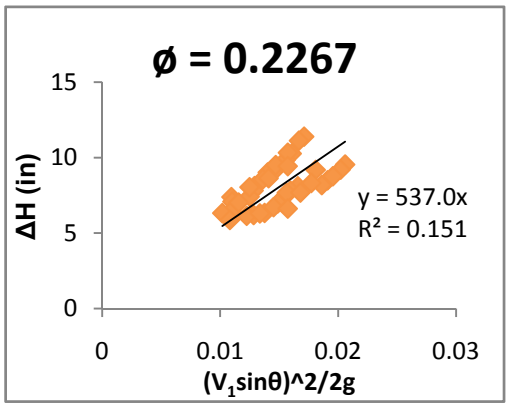

FIG. 24. Second Half of the Data set for Screens with ø = 0.2267

Conclusions

A series of experimental measurements have been carried out to study the head loss as water flows through a porous screen in an open channel. The influence factors, which include the flow rate, approaching velocity, pore size, porosity, and angle of inclination, were examined. The general trend for head loss associated with a porous

screen is: 1) as the flow rate decreases the head loss decreases and 2) as the angle of inclination decreases the head loss decreases.

When comparing the effect of the pore size with the porosity, the porosity is a more of a dominating factor in determining head loss. When the head loss is plotted against velocity head, a noticeable transition which separates different flow regimes (Darcy's or non-Darcy's flow) can be noticed. Critical Reynolds number is defined and proposed to determine where this transition occurs. For the screens with larger porosity, like the screens with a porosity of 0.4031 tested in this study, the Darcy's and non-Darcy's flow regions can be clearly identified. Two empirical formulas for the determination of head loss have been developed. For the screens with a porosity of 0.2267, the data for the region with $R_e > R_{e_{cr}}$ still support the non-Darcy's flow condition with head loss being propositional to velocity square. However, for the region $R_e \leq R_{e_{cr}}$, the flow condition as a Darcy's flow is inconclusive. More tests will be needed to re-examine the flow condition.

Future Study

A more thorough investigation will be needed to better understand the relationship between head loss and porosity. Based on experiments performed in this study, more tests on screens with various porosities (e.g. six to seven different porosity combinations) and fixed thickness (at least 0.075 inch) should be carried out to obtain better correlation between the head loss and velocity head for different porosity screen. The relationship between critical Reynolds number and porosity can be established. The

data can also be applied to develop a series of empirical formulas as shown in Equations (9a) and 9(b) to further the prediction of the head loss for a given perforated screen.

Acknowledgments

The research study described herein was sponsored by the National Science Foundation under the Award No. EEC-0649163. The opinions expressed in this study are those of the authors and do not necessarily reflect the views of the sponsor.

References

Forchheimer, P. (1901), "Wasserbewegung Durch Boden." Z Ver *Deutsch Ing*, Vol. 45, pp 1782-1788.

Venkataraman, P. and Rao, P.R.M. (1998), "Darcian, Transitional, and Turbulent Flow Through Porous Media", J. of Hydraulic Engineering, ASCE, Vol. 124, pp. 840-846.

Wang, K.H. (2004), *Screen Head Loss Tests*. Final Report submitted to Headworks, Department of Civil and Environmental Engineering, University of Houston.

Yeh, H.H. and Shrestha, M (1989), "Free-surface Flow Through Screen", J. of Hydraulic Engineering, ASCE, Vol. 115, pp. 1371-1385.

Appendix I. Nomenclature

A	=	Cross-sectional area of porous medium
A_1	=	Cross-sectional area of upstream flow
A_2	=	Cross-sectional area of downstream flow

d	=	Diameter of pores in screen
g	=	Gravitational Acceleration
L	=	Length of porous medium
Q	=	Flow rate
V	=	Average Velocity (flow rate per unit area)
S_L	=	Length of screen submerged in flow
V_1	=	Upstream velocity
V_2	=	Downstream velocity
Y_1	=	Upstream depth
Y_2	=	Downstream depth
θ	=	Angle of screen inclination
$\emptyset$	=	Porosity
k	=	Intrinsic Permeability
ν	=	Kinematic viscosity
P_a	=	Pressure at upstream of a porous medium
P_b	=	Pressure at downstream of a porous medium
ΔH	=	Head loss
∇P	=	Pressure gradient along the flow direction

Appendix II. Free-Surface Profiles as Water Flows through a Screen for Various Test Cases

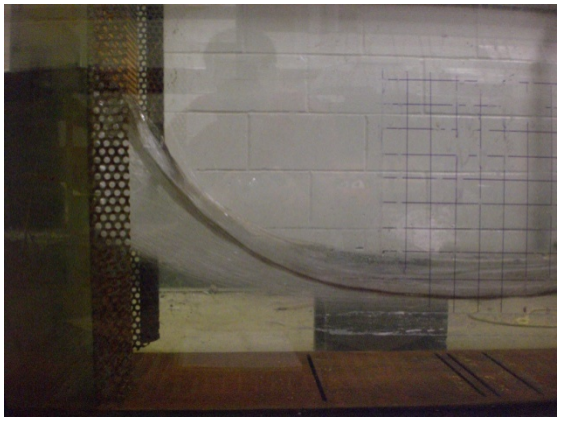

a) 1/4" Screen at 90º

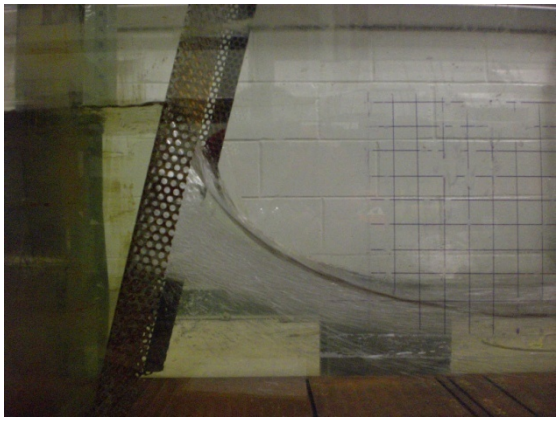

b) 1/4” Screen at 75º

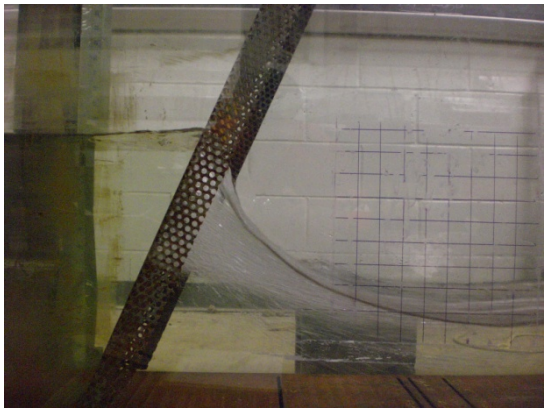

c) 1/4” Screen at 68º

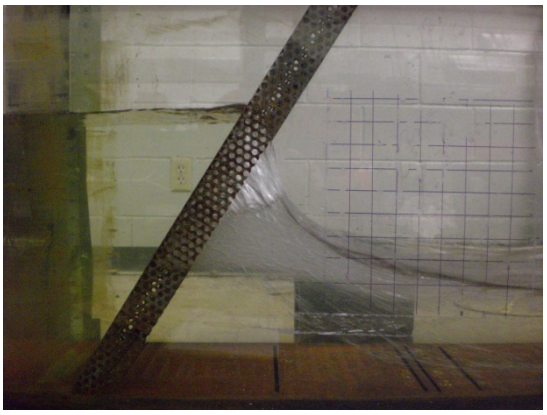

d) 1/4” Screen at 59º

FIG. 26. Water Surface Profile View of 1/4” Screen at 2.0-cfs

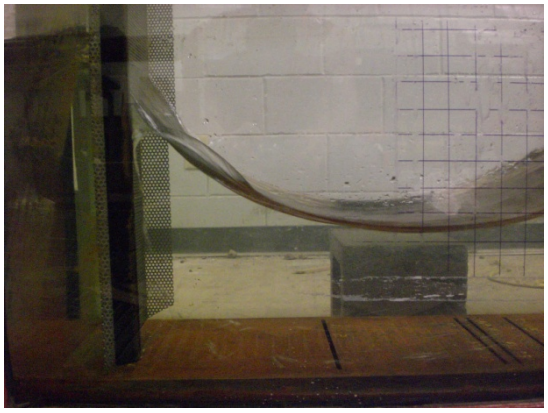

a) 1/8” Screen at 90º

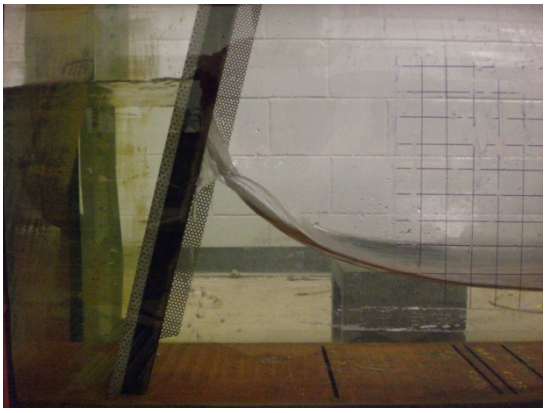

b) 1/8” Screen at 75º

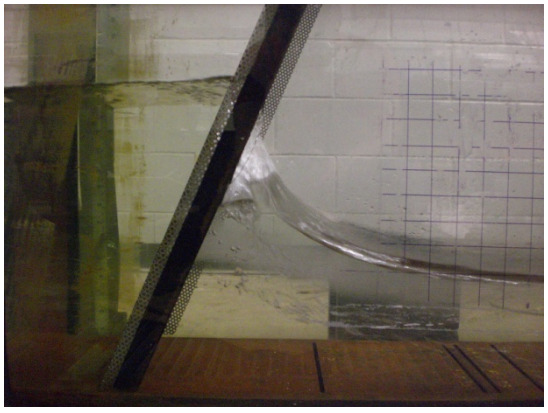

c) 1/8” Screen at 68º

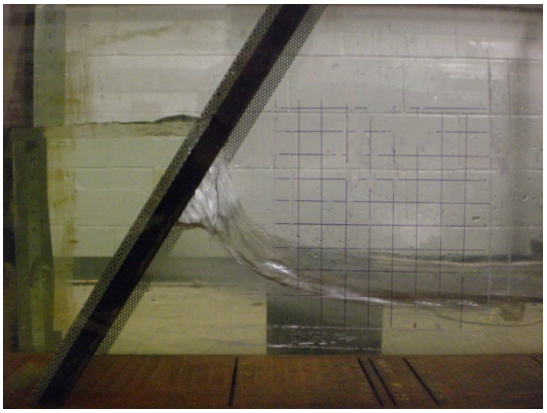

d) 1/8” Screen at 59º

FIG. 27. Water Surface Profile View of 1/8” Screen at 2.0-cfs

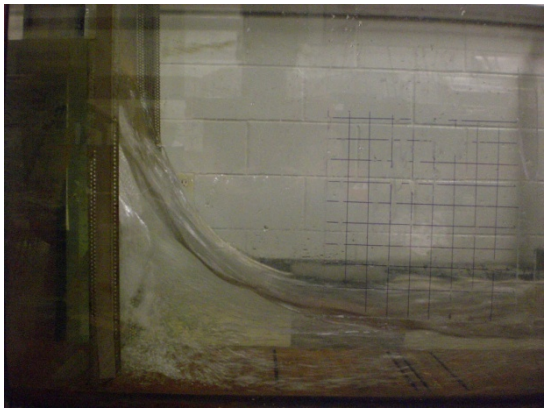

a) 3/32” Screen at 90º

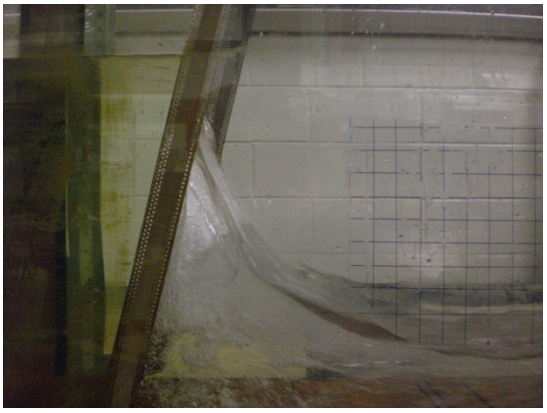

b) 3/32” Screen at 75º

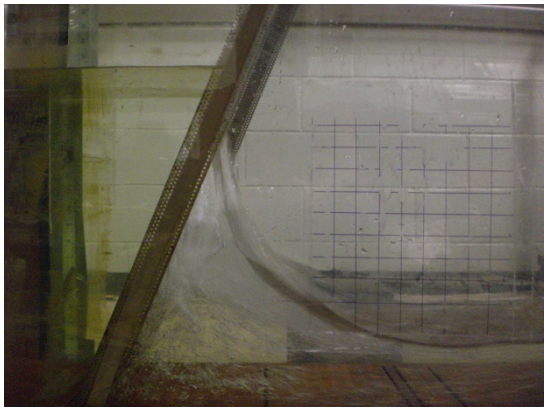

c) 3/32” Screen at 68º

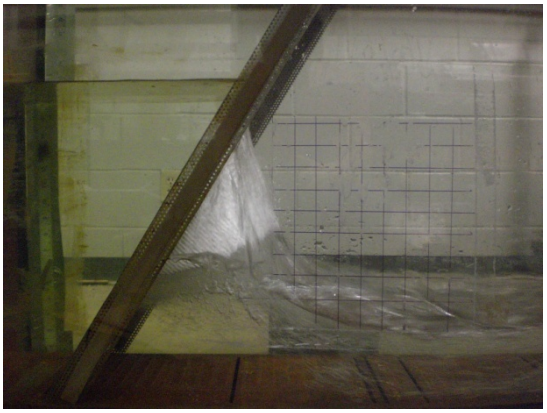

d) 3/32” Screen at 59º

FIG. 28. Water Surface Profile View of 3/32” Screen at 1.4-cfs

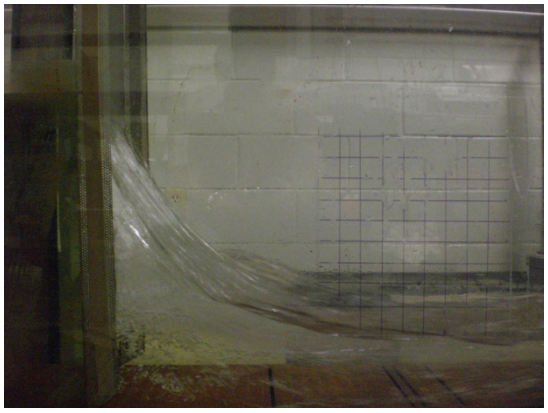

a) 1/16” Screen at 90º

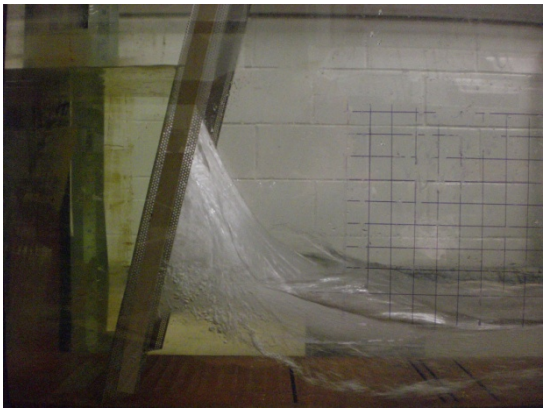

b) 1/16” Screen at 75º

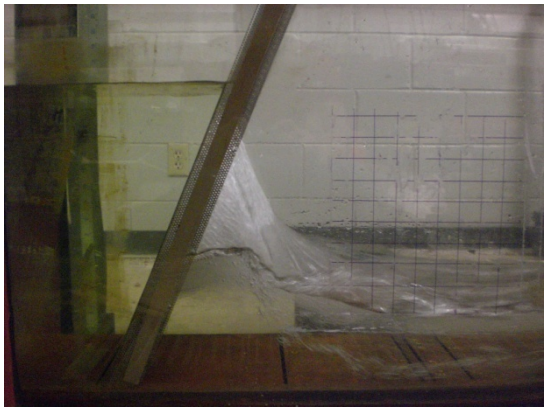

c) 1/16” Screen at 68º

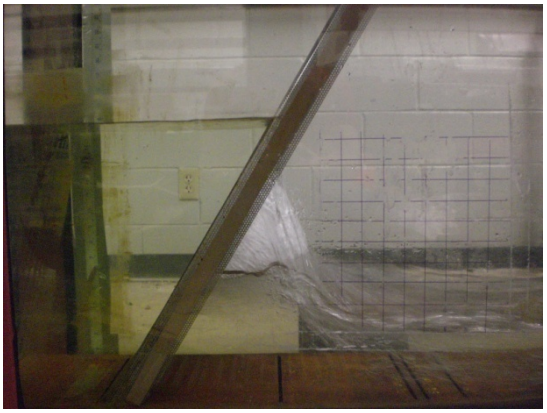

d) 1/16” Screen at 59º

FIG. 29. Water Surface Profile View of 1/16” Screen at 1.4-cfs